Egypt. J. Chem. **Vol. 68,** No. 10 pp. 141 - 155 (2025)

Egyptian Journal of Chemistry

http://ejchem.journals.ekb.eg/

Doping-Free PSf/TiO_2 Nanocomposite Membrane for Enhanced UV-Driven Photocatalytic Degradation of Ofloxacin

N.K. Abdelghany*, **M.M. Galal**[b], **H. Abd-Elhalim**

Sanitary & Environmental Engineering Division, Faculty of Engineering, Cairo University, Giza 12613, Egypt

Abstract

Pharmaceutical micropollutants are causing major concerns in water and wastewater quality. Conventional wastewater treatment plants (WWTPs) barely remove these residues effectively. In this study, a new attempt for effective ofloxacin (OFL) degradation from synthetic wastewater using doping-free polysulfone/titanium dioxide (PSf/TiO_2) nanocomposite membranes is introduced. The degradation process was enhanced by UV-driven photocatalytic process at different TiO_2 loadings (1, 3, and 5 wt%). Successful TiO_2 nanoparticle incorporation was confirmed through FTIR, TGA, SEM-EDX, and XRD analysis. Multiple parameters impact was examined, including OFL solution pH (2, normal distilled water (6), and 10), OFL initial concentrations (3, 5, 7, 10, 30, 50, and 70 mg/L), and time of UV exposure (30, 60, 180, and 240 min). PSf/TiO_2 (5 wt%) nanocomposite membrane yielded 100% OFL removal in real wastewater and exhibited the highest degradation rate of 90% for 10 mg/L OFL concentration in synthetic wastewater. Pseudo-second-order kinetics is the model that has demonstrated the best adsorption mechanism for lower initial concentrations of OFL, while Pseudo-first-order kinetics best fits higher concentrations.

Keywords: Advanced oxidation processes; Ofloxacin;Photocatalysis; Polysulfone membrane; TiO_2 nanoparticles

1. Introduction

Pharmaceuticals (PhACs) have been identified as emerging pollutants affecting water quality, despite being present in only trace amounts (ng/L to µg/L) in water-based ecosystems [1–4]. Such low levels can still harm aquatic organisms [5]. The main pathways for PhACs in the environment include illegal waste dumping, industrial wastewater, medical effluent, livestock excretion, and domestic wastewater treatment plants (WWTPs) [6–8]. Concerns about PhACs are amplified by the growing threat of antimicrobial resistance (AMR), where bacteria and viruses develop resistance to widely used drugs due to their presence in medical facilities and municipal wastewater (WW) [9].

Antibiotics are a type of pharmaceuticals frequently detected in aquatic environments, and they are used for the treatment of infections caused by pathogens in both humans and animals [10]. Recently, excessive antibiotic use was linked with higher mortality rates among COVID-19 patients, highlighting the potential dangers of pharmaceuticals accumulating in the environment [1]. A significant category of antibiotics extensively used in animals and humans are fluoroquinolones (FQs), which destroy bacteria by disrupting the production of DNA replication [11,12]. However, a significant portion (20-80%) of fluoroquinolones remain biologically active, ending up in WW and potentially harming aquatic life [13]. Ofloxacin (OFL), of all FQs, has been identified as a key target compound [14] that is not fully metabolized by humans and animals' bodies, causing potential risks [7,12]. Studies revealed various concentrations of OFL in treated effluents worldwide, ranging from 10 ng/L in freshwater environments to 1800 ng/L in municipal wastewater, with even higher levels reported near pharmaceuticals manufacturing plants up to 55 g/L [13,15].

Conventional WWTPs are ineffective at completely removing pharmaceuticals [16,17]. Based on previous studies in Egypt, Ouda et al. (2021) and Badawy et al. (2009) [18,19] concluded that a significant portion of these drugs remains in treated WW. Wastewater treatment can employ various physical, biological, and chemical methods to remove pharmaceuticals. Adsorption, membrane bioreactors, and conventional oxidation methods are the most applied physical, biological, and chemical methods, respectively [20]. However, these methods do not offer the expected removal efficiency relative to their high cost and associated generation of toxic residuals, which hinders their widespread use [21,22]. This necessitates the development of alternative methods that are efficient, environmentally friendly, and cost-effective [23].

Advanced oxidation processes (AOPs) are considered a promising approach for pharmaceuticals removal from wastewater [24,25]. AOPs offer many advantages including, strong oxidation ability to degrade pollutants completely, minimal secondary pollution formation, and the potential for enhanced performance with nanocatalysts. AOPs generate hydroxyl radicals (OH•) that efficiently oxidize complex organic pollutants into harmless byproducts [23,26]. One specific AOP, photocatalysis, relies on this principle [27–29]. TiO_2 is a popular photocatalyst due to its effectiveness, affordability, environmental safety, and chemical and biological stability. There are three known crystal forms of TiO_2: brookite, anatase, and rutile. Among these, the anatase phase exhibits the highest photocatalytic activity [30,31]. The wide band gap of 3.2 eV in TiO_2, allows it to be triggered by UV-light with a very short wavelength (below 387 nm). TiO_2 generates electron-hole ($e^- – h^+$) pairs that cause a series of reactions with water and surface hydroxyl ions (OH^-). These reactions produce (OH•) responsible for degrading organic

---

*Corresponding author e-mail: Nervana.201920647@eng-st.cu.edu.eg.; (Nervana Khamis Abdelghany).

Received date: 22 December 2024, Revised date: 20 February 2025, Accepted date: 24 February 2025
DOI: 10.21608/ejchem.2025.344533.10989

pollutants such as OFL [26,28,32,33]. The degrading mechanism of the photocatalytic process by TiO_2, involving both oxidation and reduction reactions, can be expressed by the following reactions [34]:

Electron-hole pair formation:

$$TiO_2 + h\nu \rightarrow TiO_2\ (e^-_{CB} + h^+_{VB}) \quad (1)$$

Water dissociation:

$$H_2O \rightarrow H^+ + OH^- \quad (2)$$

Oxidation reaction:

$$OH^- + h^+_{VB} \rightarrow \text{hydroxyl radical } (OH\bullet) \quad (3)$$

Reduction reaction:

$$\text{Oxygen } (O_2) + (e^-_{CB}) \rightarrow \text{superoxide radical anion } (O_2\bullet^-) \quad (4)$$

Protonation of superoxide:

$$O_2\bullet^- + H^+ \rightarrow OOH\bullet \quad (5)$$

Hydroperoxyl-oxygen reaction:

$$OOH^\bullet + O_2 \rightarrow H_2O_2 \quad (6)$$

However, some drawbacks have been reported with the use of TiO_2 in its powder form. These include the possible coagulation of the unstabilized nanoparticles, which can hinder the active sites from light absorbance and hence reduce their catalytic activity. Also, the narrow photocatalytic wavelength and limited ability to absorb visible light restrict the application of TiO_2 to organic pollutants [35]. Other drawbacks include: high cost, energy consumption, and time consumed during the TiO_2 recovery process [36].

Some researchers have recommended using a suitable support media, thereby increasing the photocatalyst's surface area and the adsorption's efficiency in addition to eliminating the ordinary filtration process conventionally required for TiO_2 recovery [36]**.** Photocatalytic support materials such as polyvinylidene difluoride (PVDF), polysulfone (PSf), polyacrylonitrile (PAN), polyethersulphone (PES), and cellulose acetate (CA) have been used for a variety of polymers [36]. TiO_2-polyethersulfone films were used for the degradation of 10 mg/l of acetaminophen in an aqueous solution achieving an 80% maximum degradation efficiency [36]. It is worth mentioning that TiO_2 also improved both hydrophilicity and water permeability, yielding further anti-fouling characteristics of these membranes [36].

To enhance the photocatalytic activity of TiO_2 and improve the efficiency of visible light absorption, recent applications suggested the modification of TiO_2 particles by doping with metals, nonmetals, semiconductors, or even carbon-based materials [37–41]. Kaur et al. (2021) [37] used copper-doped TiO_2 nanoparticles (NPs) for OFL removal and achieved about 72% degradation. Bhatia et al. (2016) [42] doped TiO_2 with bismuth and nickel and achieved 86% degradation of OFL from an aqueous solution at pH 3 within 6 hours. Other researchers used cobalt, nitrogen-doped composite nanofibers, and even silver to improve their performance in removing a range of other pharmaceutically active compounds from water [39,40,43]. Although doping methods were applied to enhance the absorption of visible light, there are some disadvantages associated with these methods including: thermal instability, cost-effectiveness, and short-term efficiency issues [35].

In this research, a novel attempt to test the performance of doping-free TiO_2 nanocomposite membranes for enhanced photocatalytic degradation of OFL in synthetic wastewater under UV-light is presented. The proposed method combines the advantages of both nanocomposite membranes and the advanced oxidation process, providing an environmentally safe, low-energy, low-equipment, and comparably cost-effective option. A simple phase inversion method was used for the fabrication of flat sheets of a PSf polymer-based matrix including TiO_2 NPs. This approach directly incorporates varying TiO_2 NPs loadings into the PSf polymer matrix during membrane fabrication. This eliminates the need for additional dopants, potentially reducing costs, while efficiently removing OFL from water. An assessment of the impact of operational parameters was also conducted, considering the initial OFL concentration, solution pH, and the kinetics of OFL elimination.

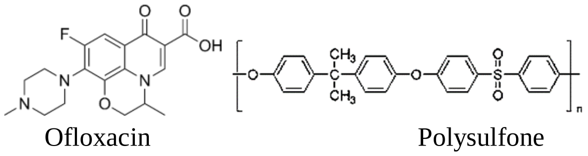

Figure 1: The chemical composition of OFL and PSf.

2. Experimental (Materials and Methods)

2.1. Materials

TiO_2 (P25, 80% anatase, 20% rutile, CAS Number: 13463-67-7) utilized in this study was provided from Sigma Aldrich, Germany. Polysulfone pellets with molecular weight (Mw: 35,000 g/mol) purchased from Sigma-Aldrich (Denmark) were used in this study. The PSf polymer acted as the membrane polymer base, while the solvent dimethylformamide (DMF) with 99.8% purity and a viscosity of 0.96 cP at 25 °C), was purchased from Sigma-Aldrich Co. (Germany). OFL ($C_{18}H_{20}FN_3O_4$), a widely used second-generation FQ antibiotic with an Mw of 361 g/mol and purity (≥98%), was sourced from EIPICO, Egypt, for this study. Figure. 1 presents the chemical structures of OFL and PSf..

2.2. PSf/TiO_2 nanocomposite membranes preparation

In this study, flat sheets of PSf/TiO_2 nanocomposite membranes were manufactured using phase inversion method in a typical synthesis procedure. This method involved creating casting solutions with 25% PSf (by weight) and varying amounts of TiO_2 NPs (0%, 1%, 3%, and 5%) dissolved in DMF solvent. The polymer solution's PSf concentration remained constant at 25 wt%. This kept the total combined weight percentage of DMF solvent and TiO_2 NPs at 75 wt% as per typical casting solutions prepared for asymmetric nanocomposite membrane fabrication by the Kesting phase inversion process [44]. Additionally, this specific ratio of PSf to solvent/nanoparticles is known to promote finger-like structure development within the membrane morphology. Three flat sheets were manufactured for each PSf/TiO_2 concentration. The nanocomposite membrane sheets were cut into square sheets (16 cm^2) to be used through the study experiments. Table 1 presents the different concentrations of TiO_2 used per membrane surface area for performing the experiments. For each TiO_2 concentration (1 wt%, 3 wt%, and 5 wt%), 3 separate membrane sheets were fabricated in which their total cumulative surface area was calculated.

2.3. *Proposed Membrane Morphology and Characteristics*

An EDX (energy dispersion X-ray) analysis detector on a Scanning Electron Microscope (SEM) TESCAN VEGA3 was employed to investigate the membranes' morphology in cross-section as well as on their top surface. The analysis used a 20 kV accelerating voltage and a 14–1,000,000x magnification at 1.50 kx for membrane cross-section and 2.00 kx for membrane top surface. This investigation was made to determine the dispersion and aggregation of TiO_2 NPs within the membrane. Liquid nitrogen was used to immerse the membranes, and after freezing, the membranes were broken for cross-sectional studies. Using Nicolet iS10 Fourier transform infrared spectroscopy (FTIR), it was possible to ascertain the chemical functional groups present in the nanocomposite membranes. X-ray diffraction (XRD) analysis was used to verify the presence of nano titania in the PSf polymer matrix. A D/max-rB diffractometer was used to record the membranes' XRD patterns. The device used copper Kα radiation (wavelength of 0.15405 nanometers) with a monochromator made of graphite. The operating conditions were 50 mA current and 50 kV voltage. The scan range was from 10 to 80 degrees. A thermal gravimetric analyzer (TGA) from Perkin Elmer (TGA7) was used to determine the thermal characteristics and stability of both PSf and PSf/TiO_2 nanocomposite membrane samples. The prepared samples were scanned under a nitrogen environment and heated to a temperature of 10 ° Celsius per minute, starting at atmospheric temperature and increasing up to 900 °C. Using a wavelength of ($\lambda = 294$ nm), a Shimadzu UV-1800 ultraviolet spectrophotometer was employed to measure the beginning and final concentrations of OFL in the solution.

Table 1: TiO_2 concentrations per surface area.

TiO_2 concentration in weight % (wt%)	Relative TiO_2 concentration in (mg)	Total area of 3 membrane sheets (cm^2)	TiO_2 concentration per each (16 cm^2) surface area in (mg)
1	50 mg	1,395cm^2	0.57
3	150 mg	1,395cm^2	1.72
5	250 mg	1,274cm^2	3.14

2.4. *Photocatalysis experimental procedures*

Batch photocatalysis experiments were performed for the degradation of OFL. A plastic container with dimensions (length 9 cm, width 9 cm, and height 3 cm), was filled with a 50 ml solution of known concentration of OFL and diffused into distilled water to reach the required initial concentrations. The nanocomposite membranes were then placed inside the solution at 25°C ± 2°C in suspension mode. Subsequently, the container was fully covered to ensure complete darkness. It was then shaken on an orbital shaker (OVAN-OM10E) at 70 rpm for 30 minutes without irradiation to attain equilibrium between adsorption and desorption. The system's radiation source was a 40-watt UV-A lamp (wavelength range 315-400 nm) installed directly above the containers filled with OFL solution, at a total distance of 10 cm from the container's bottom, for an exposure duration of 240 min. To achieve the required starting pH, a pH meter (EcoSense series pH1000A) was utilized and the solution was adjusted by adding 0.1 N (NaOH, ≥95% purity) or 0.1 N (HCL, 36.0% purity), both from (ADVENT). Figure 2 presents the schematic diagram for the experimental setup.

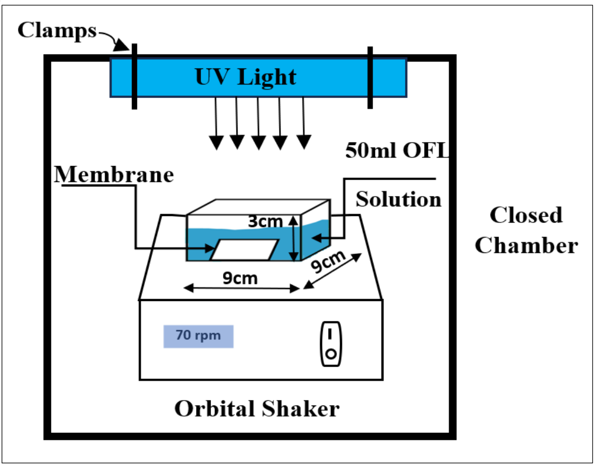

Figure 2: Schematic diagram of the experimental setup.

Initially, a 3 mg/L OFL concentration was studied at different solution pH levels (2, normal distilled water (6), and 10) to determine the effect of the solution's pH. Then, the study of TiO_2 catalyst loading effect was performed by increasing the surface area of the manufactured nanocomposite membranes PSf/TiO_2 (1 wt%, 3 wt%, and 5 wt%). In light of these findings, 4 membranes with a total catalyst loading of 12.56 mg/TiO_2 were chosen to degrade different OFL initial concentrations of 3,5,7,10,30,50, and 70 mg/L for 240 min. The drug solution was sampled at fixed time intervals, with a sample volume of 5 mL. The influence of contact time on reaction rate (kinetics) was studied at the highest pH value and TiO_2 concentration, where the final OFL concentrations were measured at various contact times (10-240 min). After each experiment, the nanocomposite membranes were repeatedly washed with distilled water to be reused in subsequent experiments. To ensure that the results were uniform and reliable, all tests were carried out in duplication, and the mean results were used. The degradation performance was determined using the following equation:

$$\text{Degradation efficiency (\%)} = \left(\frac{C0-Ct}{C0}\right) \text{X } 100 \qquad (7)$$

where C_0 (mg/L) is the initial OFL concentration and C_t (mg/L) represents the concentration at time (t).

3. Results and discussion

3.1. Characterization

Figures (3a - d) demonstrate the cross-sectional morphologies within the nanocomposite membranes. The cross-sectional view is shown in Figure 3a of the neat PSf membrane, where clear macropore structures are observed. Figures (3b - d) demonstrate that an increase in TiO_2 filler's concentration gradually converts macropores in the membrane's support layer at lower TiO_2 loadings to finger-like pores. The asymmetric membranes' finger-like morphology is a characteristic that includes a porous underlayer and an arrangement that resembles a finger in its cross-section. The conversion from macropores to finger-like pores is due to the interfacial stress between PSf and catalyst, as it is released by the development of interfacial pores. The macropores grow larger at low TiO_2 filler's concentration (1 wt%). At increasing filler's concentration (3 wt%), the size and quantity of macropores begin to diminish, while the thickness of the support layer expands as the filler's concentration rises. Finger-like structures and agglomeration of TiO_2 NPs start to occur with a further increase in filler's concentration (5 wt%) as shown in Figure 3d and indicated in the red circles. These results show that the addition of TiO_2 NPs significantly affects the membrane shape. Hence, it is concluded that the addition of inorganic fillers changes the mechanism of composite membranes. These observations are in agreement with two studies by Zhang et al. (2013) and Yang et al. (2007) [45,46].

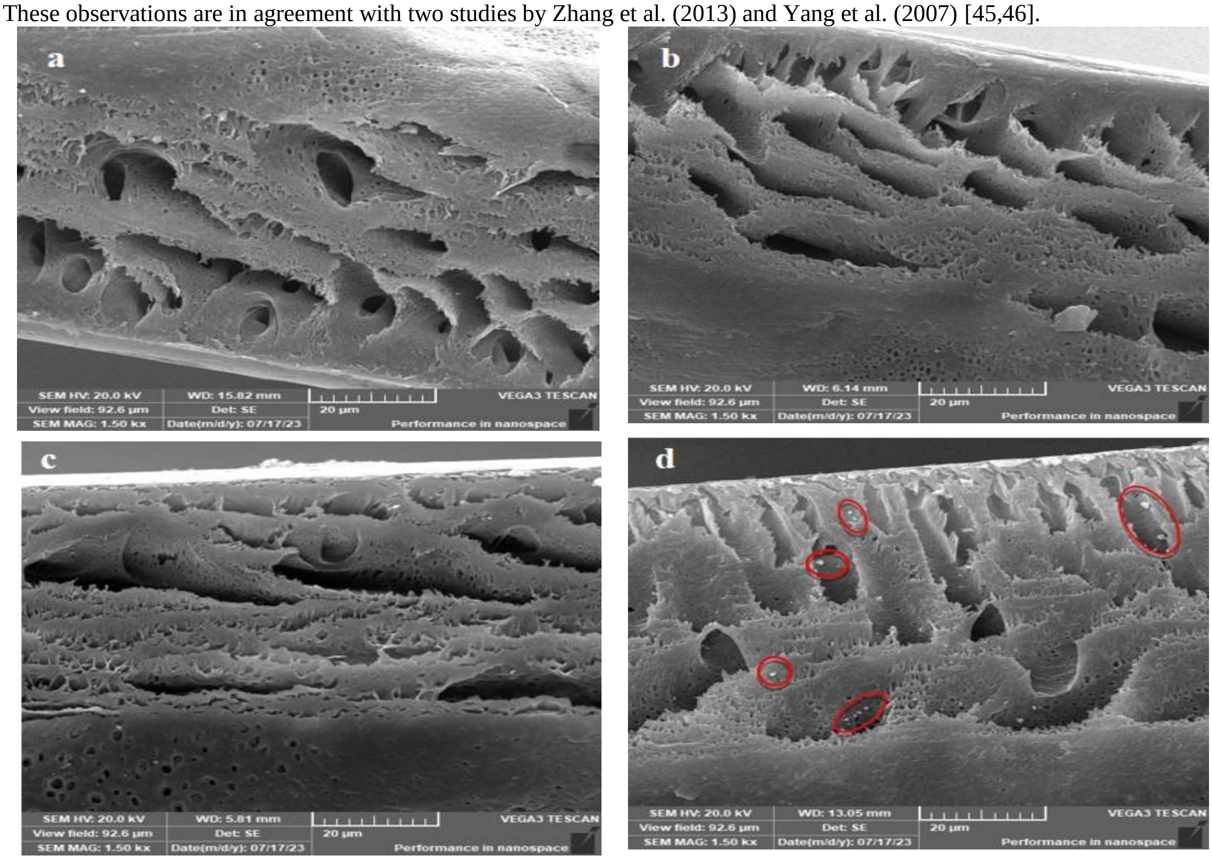

Figure 3: SEM images of (a) neat PSf, (b) PSf/TiO_2 1 wt%, (c) PSf/TiO_2 3 wt%, and (d) PSf/TiO_2 5 wt% cross-sections.

Figures (4a - d) show the membrane's top surfaces. It can be concluded that the membranes with 1 wt% and 3 wt% TiO_2 filler have no visible TiO_2 NPs on their top surface. As for 5 wt% TiO_2, TiO_2 NPs agglomerates were homogenously distributed and visible on the top membrane's surface, indicated by the red circles (Figure (4d)). This observation may be explained by the TiO_2 NPs integration within the matrix of the polymer as well as the higher rate of interchange between the solvent and nonsolvent throughout the phase inversion process, which caused the TiO_2 NPs to transfer to the uppermost membrane layer. This is favorable as it makes the surface of the membrane more hydrophilic [45,47].

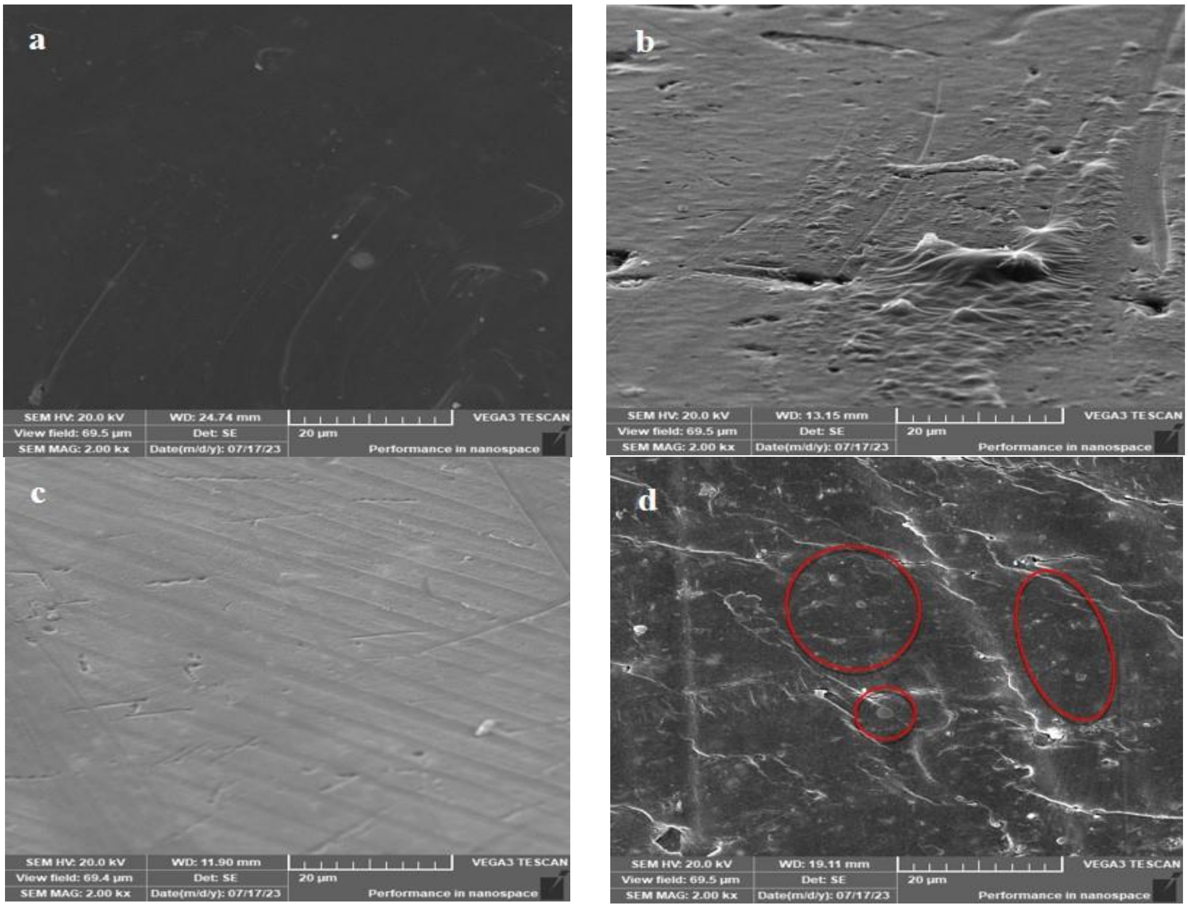

Figure 4: SEM images of (a) neat PSf, (b) PSf/TiO_2 1 wt%, (c) PSf/TiO_2 3 wt%, and (d) PSf/TiO_2 5 wt% top surfaces.

Both the PSf/TiO_2 nanocomposite membrane and neat PSf membranes' elemental compositions had been identified using the EDX analysis. The spectra revealed typical peaks for PSf polymer where carbon, sulfur, and oxygen were predominantly present in all membrane analyses. The TiO_2 NPs were firmly placed inside the PSf polymer matrix, as indicated by the appearance of an additional element peak of Ti in the EDX spectra for the for (1 wt %, 3 wt%, and 5 wt%).

Figures (5a - d) display the EDX spectrum of the neat PSf membrane and PSf/TiO_2 nanocomposite membranes.

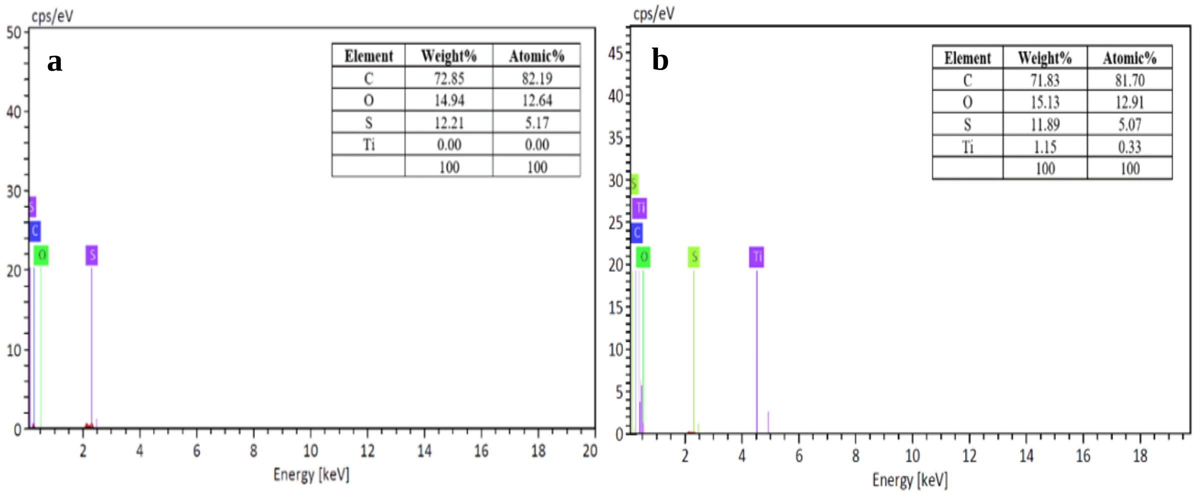

a

Element	Weight%	Atomic%
C	72.85	82.19
O	14.94	12.64
S	12.21	5.17
Ti	0.00	0.00
	100	100

b

Element	Weight%	Atomic%
C	71.83	81.70
O	15.13	12.91
S	11.89	5.07
Ti	1.15	0.33
	100	100

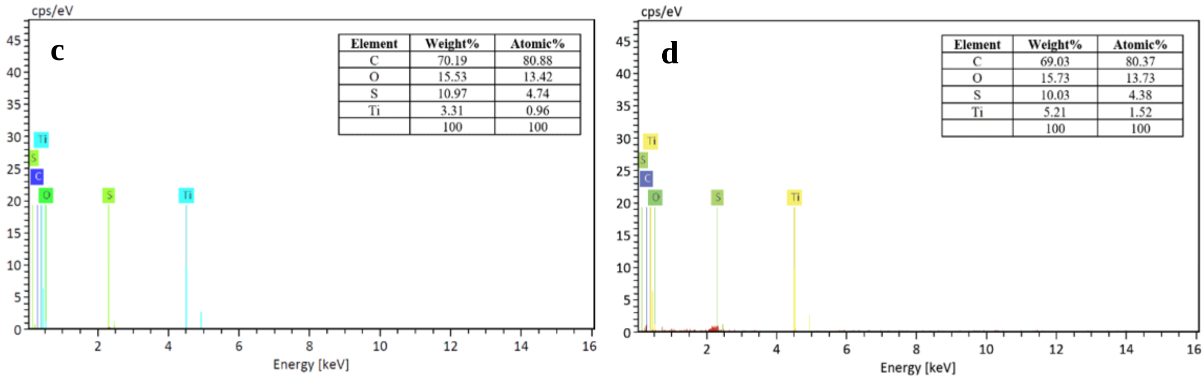

Figure 5: EDX analysis of (a) neat PSf, (b) PSf/TiO$_2$ 1 wt%, (c) PSf/TiO$_2$ 3 wt%, and (d) PSf/TiO$_2$ 5 wt%.

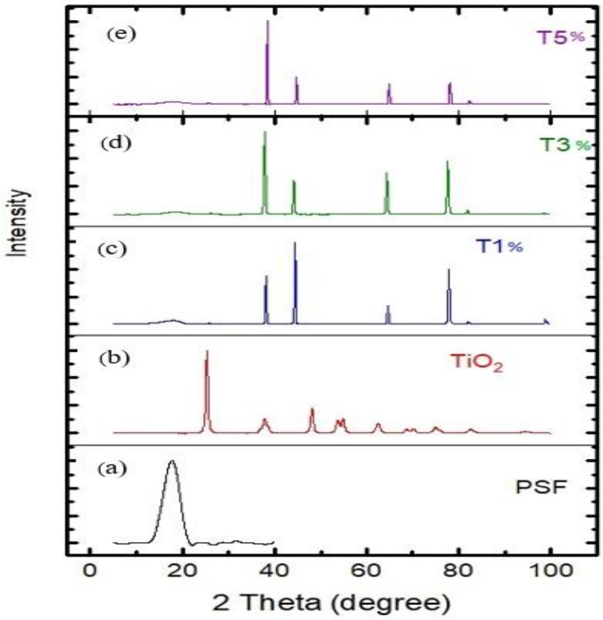

Figure 6: XRD patterns for (a) neat PSf, (b) TiO$_2$ NPs, (c) PSf/TiO$_2$ 1 wt%, (d) PSf/TiO$_2$ 3 wt%, and (e) PSf/TiO$_2$ 5 wt%.

The XRD diffraction structures of neat PSf membrane, nano-sized TiO$_2$ crystalline powders, and PSf/TiO$_2$ nanocomposite membranes, are shown in Figure 6. Peaks at $2\theta = 25.32^\circ$, 36.8° and 47.6°, 54.2°, 56.3°,62.4°, and 69.1° confirm the anatase phase of TiO$_2$ crystal powder (JCPDS Card no. 21–1272) [26,48]. The PSf/TiO$_2$ nanocomposite membrane pattern also featured crystalline distinctive peaks at $2\ \theta$ of 38.96°, 48.40°, and 65.01° These peaks were comparable to the dispersion peak of neat PSf and the typical peaks of TiO$_2$ crystal powders; their positions, however, were slightly shifted when compared to the TiO$_2$ NPs pattern. The shift of the distinctive TiO$_2$ peaks in the PSf/TiO$_2$ nanocomposite membrane implied that titania had been successfully incorporated into the membrane matrix [49]. Significantly, the PSf/TiO$_2$ nanocomposite membrane's peak intensities were greater and sharper than TiO$_2$ NPs peaks, indicating the creation of bigger crystals with higher crystallinity. Similar results were observed by Eslami et al. (2016) [27]. The samples were analyzed by Fourier transform infrared (FTIR) spectrum at wavenumbers between 4000 to 500 cm^{-1}. Neat PSf membrane, PSf/TiO$_2$ (1 wt%, 3 wt%, and 5 wt%) nanocomposite membranes, and bare TiO$_2$ NPs FTIR spectra are shown in Figure 7.

Investigating the functionalized TiO$_2$ NPs spectra, the existence of TiO and Titanium–Oxygen–Titanium bonds in the bare TiO$_2$ NPs of the produced nanocomposite membranes was demonstrated by an absorption peak located at around 500 cm^{-1}. In the 1240–1350 cm^{-1} range, there were two absorption peaks which suggested that the PSf absorbance was stretching vibrationally O=S=O. C=C in the aromatic rings of polysulfone was identified as the source of a high-intensity peak at 1575 cm^{-1}. At 2985 cm^{-1}, a minor peak for the vibratory stretch of CH$_3$ was observed. The hydroxyl groups of (O–H) exhibit symmetric and asymmetric deformed vibrations at 1365 and 1480 cm^{1} [26,47,50].

Figure 8 displays the neat PSf membrane and PSf/TiO$_2$ nanocomposite membrane thermal gravimetric analysis (TGA) graphs at different TiO$_2$ concentrations. The highest thermal stability was for pure TiO$_2$ NPs with noticeably minor weight loss. The reduction of moisture content and/or solvent evaporation from the produced membranes was demonstrated by the thermographs of each membrane sample, which revealed that the initial weight loss was detected from the ambient temperature of 400 °C. Following that, there was a significant weight loss in the 450–500℃ temperature range, which was indicative of polymer backbone breakdown. Remarkably, as the quantity of TiO$_2$ NPs increased, the nanocomposite membrane exhibited greater thermal stability, indicating an even distribution of TiO_2 NPs across the membranes [51]. The graph shows that combining TiO_2 NPs with polymer-mixed matrices and increasing their concentration enhanced thermal stability, whereas the neat PSf membrane demonstrated the least thermal stability compared to the PSf/TiO_2 nanocomposite membrane. The weight loss for the PSf/TiO_2 nanocomposite membrane and the neat PSf membrane decreased in the following sequence from highest to lowest: PSf/TiO_2 (5 wt%) nanocomposite membrane, which showed higher thermal stability than PSf/TiO_2 (3 wt%) nanocomposite membrane, followed by PSf/TiO_2 (1 wt%) nanocomposite membrane, with the neat PSf membrane exhibiting the least thermal stability. Similar findings were observed in the studies by Moradihamedani et al. (2015) and Ali et al. (2020) [50,52].

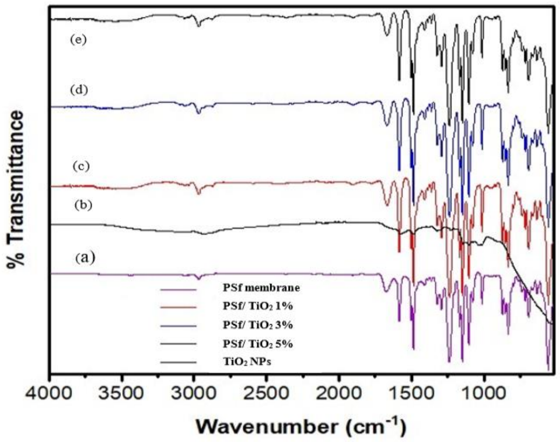

Figure 7: FTIR spectrum for (a) neat PSf, (b) TiO_2 NPs, (c) PSf/TiO_2 1 wt%, (d) PSf/TiO_2 3 wt%, and (e) PSf/TiO_2 5 wt%.

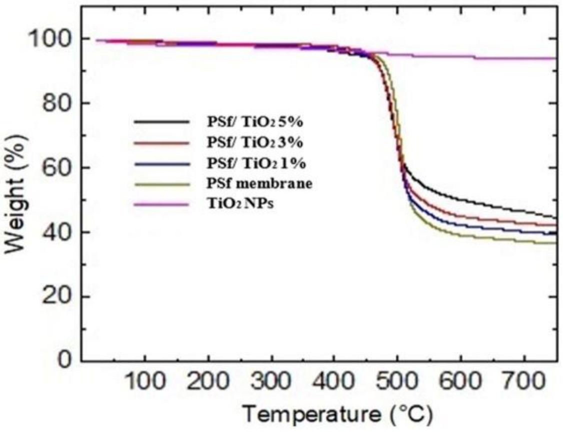

Figure 8: TGA curves of neat PSf, TiO_2 NPs, PSf/TiO_2 1 wt%, PSf/TiO_2 3 wt%, and PSf/TiO_2 5 wt%.

3.2. Kinetics Study

Using the models of Pseudo-first order (PFO) and Pseudo-second order (PSO), the linear kinetic analysis was utilized to model the photocatalytic degradation of OFL according to the following conditions (pH: normal distilled water (6), PSf/TiO_2:5 wt%, OFL: 3-70 mg/L, Temperature (*T*)= 25 °C ± 2°C, exposure time: 240 min). PFO kinetic model linear form is represented as follows [32]:

$$\mathrm{Ln}\ C_0/C_t = k_1 t \qquad (8)$$

Where the steady rate is k_1 measured as (1/min) and its duration is in (min), C_0 is the starting OFL concentration (mg/L), and C_t is the OFL concentration (mg/L) at duration t. When $\ln(C_0/C_t)$ is plotted against t, an uninterrupted line having a slope equal to k_1 is produced. An expression for the PSO kinetic linear form is as follows [32]:

$$1/C_t - 1/C_0 = k_2 \qquad (9)$$

A linear graph with a slope of k_2 is obtained by graphing $1/C_t - 1/C_0$ versus t. The graphs shown in Figures (9a and 9b) indicate that the PSO kinetic model for OFL's regression coefficient (R^2) values best fits lower OFL concentrations of 3, 5, 7, and 10 mg/L. In contrast, higher OFL concentrations of 30, 50, and 70 mg/L best fitted the PFO kinetic model. This can be explained by that at lower OFL concentrations, more available active sites for hydroxyl radicals can be found on the membrane's surface, hence increasing the rate of adsorption. At higher OFL concentrations, fewer available active sites for hydroxyl radicals can be found, leading to a slower adsorption rate, as clarified by an earlier study by Chijioke-Okere et al. (2021) and Simonin et al. (2016) [36,53]. Additionally, it was observed that the steady rate K_1 decreased from 0.0056 to 0.0015 min^{-1} at a duration of t = 240 min when the OFL concentration increased from 30 to 70 mg/L, respectively. These results are similar to those obtained by Ahmadi et al. (2017) and Jorfi et al. (2016) [32,54].

3.3. Impact of the initial solution pH

The pH affects the photocatalyst's surface characteristics, its electrical charge, the dissociation of pollutants, and the chemical composition of the pharmaceuticals in the solution. Therefore, it is an essential parameter for the photocatalytic procedure and can substantially impact its outcome. By adjusting the solution pH values (2, normal distilled water (6), and 10) at a fixed catalyst amount using one PSf/TiO_2 nanocomposite membrane sheet 5 wt% (3.14 mgTiO_2) with relative surface area 16 cm^2 to degrade 50 mL of drug with concentration 3 mg/L, pH's impact on the efficiency of OFL removal was investigated. As shown in Figure 10, the maximum rate of photocatalytic degradation for OFL in standard distilled water at pH value (6) was 63%. Previous studies recommended the use of pH 2 with similar TiO_2 nanocomposite membranes as indicated by Mohamed et al. (2018) and Şerife Parlayıcıa et al. (2015) [55,56]. These studies demonstrated that low pH conditions are feasible for photocatalytic applications involving similar nanocomposite membranes.

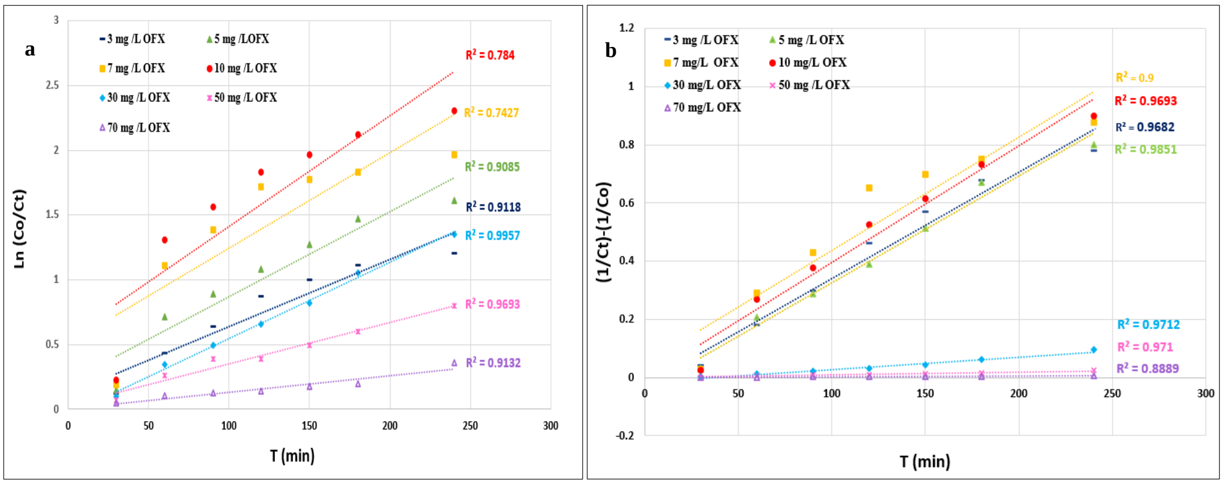

Figure 9: Kinetic study for OFL photocatalytic degradation (pH: normal distilled water (6), PSf/TiO$_2$: 5 wt%, OFL: 3-70 mg/L, *T*= 25 °C ± 2°C, irradiation time: 240 min) where, (a) PFO model, and (b) PSO model.

The anatase TiO$_2$ point of zero charge (pzc) is at pH 6. Accordingly, the catalyst layer has a positive charge in pH<6 (acidic media) and is negatively charged in pH>6 (basic medium). When the pH is below pKa$_1$ (6.05), OFL has a positive charge; when the pH is higher than the pKa$_2$ (8.11), it is negatively charged; and when the pH is between the pKa$_1$ and pKa$_2$, it is neutral [7,13,57,58]. It is not recommended to use pH 2 or 10 for adsorption of OFL on the nanocomposite membrane's top layer owing to the electrical repulsion generated by the compound's charges and the catalyst having a common sign. At the pH of normal distilled water (6), the drug and the catalyst molecule are neutral and do not repel each other. These outcomes are consistent with the study's findings, which showed that pH 6 produced the highest removal efficiency for OFL.

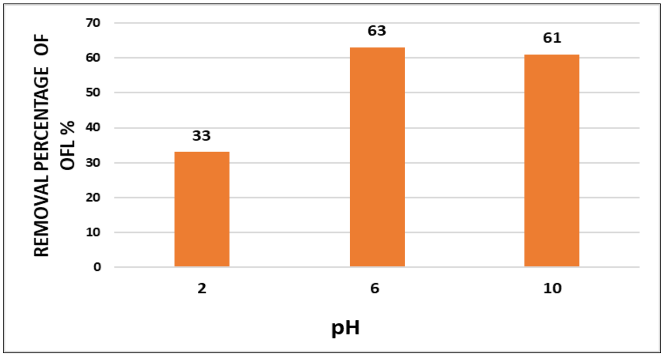

Figure 10: OFL removal at pH values of 2, normal distilled water (6), and 10 at catalyst dose 5 wt% (1 membrane sheet), OFL= 3 mg/L.

3.4. Catalyst concentration and surface area effect on degradation efficiency

The impact of catalyst concentration on photocatalytic degradation of OFL was investigated using one membrane sheet of surface area 16cm^2 for each chosen concentration (5 wt% (3.14 mgTiO$_2$), 3 wt% (1.72 mgTiO$_2$), and 1 wt% (0.57 mgTiO$_2$)). The highest photocatalytic degradation of 3 mg/L OFL was achieved by using the nanocomposite membrane with the highest amount of catalyst 5 wt% (3.14 mgTiO$_2$) at pH 6 as presented in Figure 11. Increasing the amount of TiO$_2$ catalyst improved the photocatalytic decomposition rate for OFL from 48% to 63%. The increased quantity of sites that are active on the nanocomposite membrane's top layer could be the reason for this improvement [32].

The impact of increasing the surface area of the nanosheets with increasing the concentration of TiO$_2$ catalyst was also investigated. Increasing the number of nanosheets (6.8 mgTiO$_2$ using two membranes with an overall membrane surface area of 32 cm^2 and 12.56 mgTiO$_2$ using four membranes having a total surface area of 64 cm^2) was carried out in a series of experiments with the same previous setup. The photocatalytic removal rate of 3 mg/L OFL improved from 63% to 70% when the amount of the catalyst added and the surface area was increased, as shown in Figure 12. In line with the results of Koe et al. (2020) [28], the study outcomes highlighted a direct relation between the quantity of the sites that are active in the exposed membrane surface and the quantity of the catalyst, as well as the surface area of the nanocomposite membrane sheet. In addition, it should be noted that enhancing the loading of the catalyst offers improved binding sites for the adsorption of the drug compounds on the membrane's surface. The observed improvement in degradation was possibly from the larger levels of reactive hydroxyl radicals produced as more electrons and hole pairs were generated on the membrane's surface [59].

Considering the previous outcomes, 4 membrane sheets of PSf/TiO$_2$ (5 wt%) nanocomposite membranes were chosen for the following experiments.

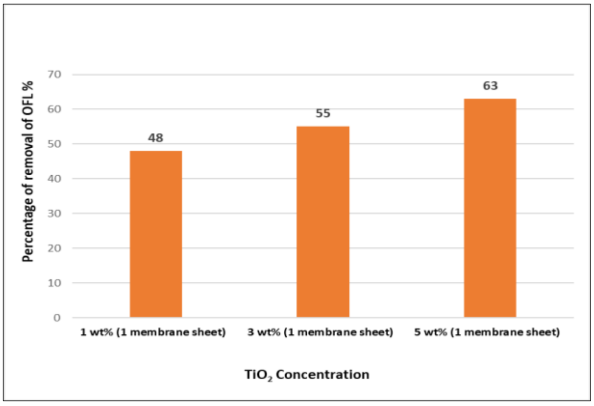

Figure 11: Impact of catalyst concentration (1, 3, and 5 wt%) on the 3 mg/L OFL degradation efficiency.

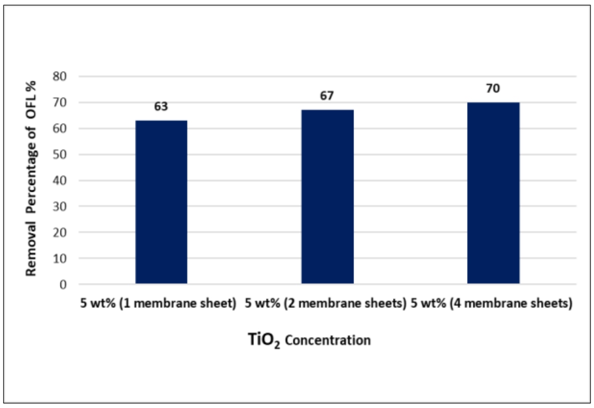

Figure 12: Effect of increasing membrane surface area (1 membrane sheet, 2 membrane sheets, and 4 membrane sheets) on the photocatalytic degradation efficiency of 3 mg/L OFL.

It is worth mentioning that based upon the earlier research by Kusworo et al. (2021) and Bilal et al. (2024) [60,61], TiO$_2$ NPs can typically improve the membrane's hydrophilicity. TiO$_2$ incorporates hydrophilic groups consisting of -COOH and -OH, which enhance the membrane's hydrophilicity. TiO$_2$ present in the casting mixture attracts water molecules into the membrane, enabling their movement along the flow channels created by the TiO$_2$ inclusion, thereby raising membrane porosity. Furthermore, Kusworo et al. (2021) and Pedersen et al. (2018) [60,62] mentioned that a greater concentration of TiO$_2$ noticeably elevates the surface energy of the membranes, resulting in them being more suitable for water contact and thus enhancing wettability. An enhanced water layer on the top surface of the membrane was formed as a result of the improved hydrophilicity brought on by TiO$_2$. Water molecules can move more easily throughout the membrane owing to that layer, which reduces the contact between contaminant particles and the membrane's polymer. Consequently, the improved membrane's hydrophilic properties enhance overall membrane efficiency [60].

3.5. Impact of the drug's initial dosage

The concentration of a certain drug affects how well it degrades by photocatalysis. Figure 13 illustrates the degradation efficiencies of OFL with initial concentrations of 3,5,7,10, 30, 50, and 70 mg/L with 4 nanocomposite membrane sheets of PSf/TiO$_2$ (5 wt%) and a total catalyst quantity of 12.56 mgTiO$_2$ under UV-light exposure. According to the obtained results, the efficiency for OFL degradation increased with increasing the initial drug concentration till it reached 90% at 10 mg/L initial concentration. Then, there was a significant decrease in the removal efficiency to 30% for 70 mg/L of OFL. One explanation for this might be that the hydroxyl radicals on the catalyst's top surface start to decrease as the starting dosage of the pharmaceutical increases.

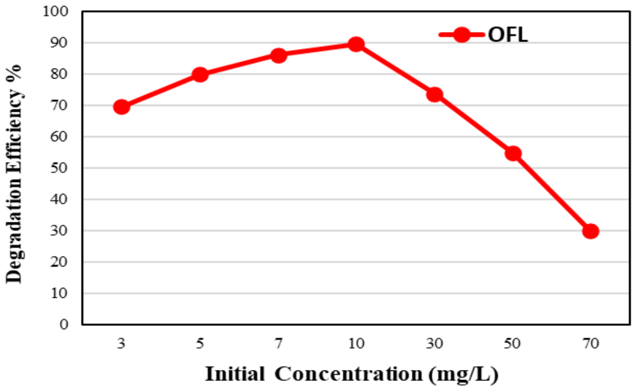

Figure 13: Effect of initial drug dosage on the efficiency of degradation at pH 6 when exposed to UV-light, TiO$_2$ concentration 12.56 mgTiO$_2$, and exposure time of 240 min.

The PSf/TiO$_2$ nanocomposite membrane will have fewer active sites available for hydroxyl radicals' adsorption when the quantity of drug molecules adsorbed on the photocatalyst surface rises. Increased quantities of adsorbed pharmaceuticals might hinder the bonding between pharmaceutical compounds and hydroxyl radicals since there would be no direct contact. Also, when drug concentration rises, more UV-light is absorbed by the drug molecules. This prevents photons from reaching the photocatalyst's surface and producing hydroxyl radicals. Additionally, as the membrane's surface is covered by the overloaded OFL, the photocatalytic degradation reaction will be less active. Chijioke-Okere et al. (2021) and Mohamed et al. (2018) [36,55] showed similar results. As a result, at high drug concentrations, the degradation efficiency gradually drops.

3.6. Impact of exposure duration

All nanocomposite membranes and OFL samples were placed on the orbital shaker in complete darkness for 30 minutes before the photocatalytic procedure. This allowed the adsorption-desorption equilibrium to attract as many OFL molecules as possible to the surface of the photocatalytic membrane to begin the photodegradation process. After that, all the membrane samples were irradiated with UV-light. Thus, electron photons reaching the membrane's surface, started an interaction between hydroxyl radicals and drug molecules. Consequently, the degradation of OFL began through the photocatalytic process. As can be observed from the results shown in Figure 14, the PSf/TiO_2 (5 wt%) nanocomposite membrane with the total amount of catalyst (12.56 mgTiO_2) was used to degrade 50 ml of different OFL concentrations (3,5,7,10, 30, 50, and 70 mg/L). High removal rates were obtained in the first 60 minutes of UV-light exposure; as a result of more available active sites and more hydroxyl radicals when the dose of the membrane catalyst increased. Until equilibrium was established after about 240 min, these active sites reported slower rates of removal, where the photocatalytic degradation rate reached the maximum OFL removal and remained almost constant after. Previous research by Dekkouche et al. (2022) and Chijioke-Okere et al. (2021) [26,36] employed PSf/TiO_2 and PES/TiO_2 nanocomposite membranes with higher catalyst concentrations (11 wt% and 14 wt%, respectively) and achieved degradation of various pharmaceuticals under UV-light exposure, they required lower pollutant concentrations (0.3-10 mg/L) and significantly longer treatment duration (420-1440 minutes). In contrast, the proposed doping-free membranes achieved comparable degradation efficiency with a lower catalyst loading and a shorter treatment time for OFL, suggesting a potentially more efficient and economical strategy.

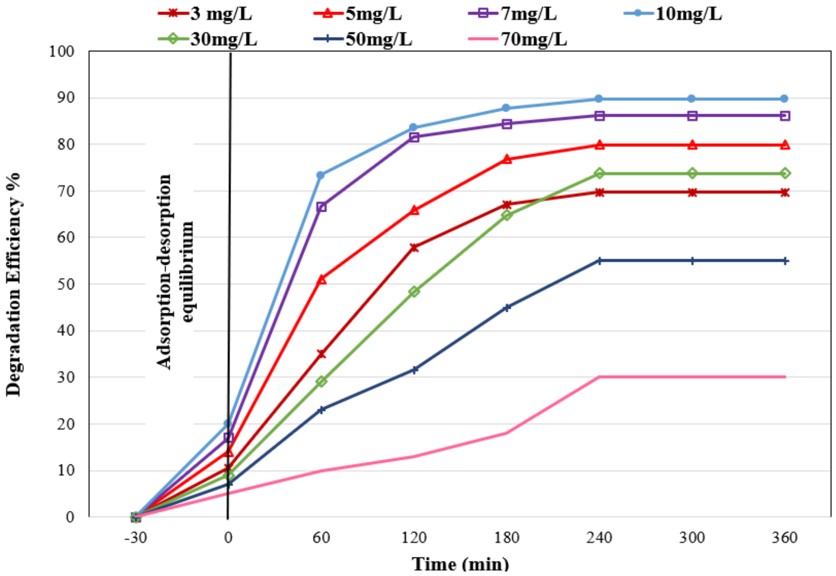

Figure 14: Impact of exposure duration on the degradation efficiency at various OFL concentrations.

3.7. Membrane removal efficiency in real wastewater

The removal of OFL from real wastewater by the PSf/TiO_2 nanocomposite membrane was investigated. As illustrated in Table 2, the real wastewater values used in this investigation were provided from the final sedimentation tank at the ZENEEN wastewater treatment plant in Egypt. According to previous findings, PSf/TiO_2 5 wt% (12.56 mg TiO_2) nanocomposite membrane showed the highest degradation performances in synthetic wastewater at 10 mg/L initial OFL concentrations with a 90% removal efficiency. The experimental conditions for real wastewater were also maintained as previously described: pH of real wastewater of 7.45, UV irradiation time of 4 hours, and ambient temperature of 25 °C ± 2 °C. To determine more accurate measurements of OFL concentration values, especially in multi-contaminant solutions such as real wastewater, high-performance liquid chromatography (HPLC) on the YL9100 HPLC system series (Korea) was used to analyze each experimental sample.

Figures (15a - c) illustrate the resultant HPLC chromatograms for three samples taken at different times during the experiment. These graphs illustrate the voltage, measured in millivolts (mV), on the Y-axis, and the retention time in minutes on the X-axis when OFL passes through the column and reaches the device's detector. The voltage represents the HPLC detector's signal output. This signal corresponds to the presence of OFL by measuring its absorption of UV radiation. High compound concentrations are indicated by higher peaks. The time of OFL detection is indicated at the top of each figure's peak. The initial concentration of OFL (C_0) before treatment, at 10 mg/L, presented the highest voltage peak on the Y-axis indicating a high concentration of OFL, as shown in Figure 15a. The second sample was taken after the first 30 minutes in complete darkness, the concentration substantially dropped to 2.346 mg/L, showing a lower peak, with a removal efficiency of 77%, as illustrated in Figure 15b. The third sample was taken after 4 hours of UV irradiation, in which a complete (100%) removal of OFL was accomplished, where no peaks were detected, indicating no presence of OFL, as shown in Figure 15c.

The obtained results indicate that the TiO_2 NPs in the membrane have excellent adsorption capability of drug molecules under dark conditions and exhibit very high photocatalytic efficiency under UV light for real wastewater contaminant removal, though complex compounds exist in real wastewater [32,63].

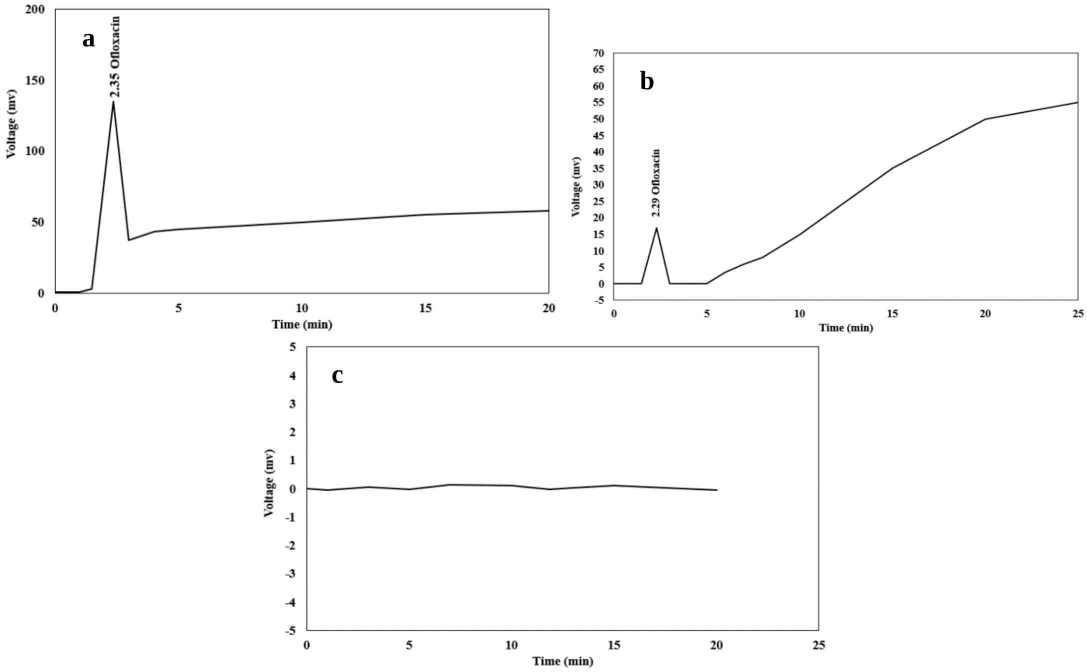

Figure 15: HPLC chromatogram of OFL concentration in real wastewater of (a) initial (C_0) concentration (10 mg/L) before treatment, (b) after the first 30 minutes in complete darkness, and (c) final concentration after treatment.

Table 2: Real wastewater values.

Parameter	Value
pH	7.45
BOD_5 (mg/L)	15.3
TS (mg/L)	435
TVS (mg/L)	237
VSS (mg/L)	11.07
TSS (mg/L)	15

3.8. Membrane stability across several cycles of reactions

The effectiveness, stability, durability, and reusability of the nanocomposite membranes for OFL degradation were investigated through six consecutive photocatalytic experiments. The same single 5 wt% membrane was used to degrade 3 mg/L OFL in 50 mL drug solution with a typical distilled water pH (6) for 240 min in each experiment. To reuse the nanocomposite membrane in the upcoming experiment, it was washed many times with distilled water after any degradation experiment and then dried in air without requiring any further recovery processes. Figure 16 indicates that the membrane was stable for the first five cycles in a row, maintaining the same photodegradation effectiveness of 63%. However, in the sixth cycle, the efficiency dropped to 35% removal. The organic compounds' adsorption onto the top membrane surface, causing the prevention of UV-light from reaching the membrane's catalytic active site, might be the cause of this drop in photodegradation effectiveness. Accordingly, the membrane requires backwashing to reversibly remove loosely attached foulants on the membrane surface hence preserving its photocatalytic activity.

In general, when comparing this study to a previous study by Singh et al. (2021) [16], which used TiO_2 doped hydroxyapatite-incorporated photocatalytic membranes for the degradation of chloramphenicol antibiotic in water, a TiO_2 concentration of 4 wt% was used to remove 50 mg/L of chloramphenicol under UV irradiation for 120 minutes, achieving a 61.59% removal. Another study by Koe et al. (2020) [28] used nitrogen and sulphur co-doped carbon quantum dots/TiO_2 photocatalytic membrane for degradation of diclofenac from water, using a large amount of TiO_2 concentration (200 mg) to remove 10 mg/L of diclofenac under UV irradiation for 120 minutes, achieving less than 62.30% removal. In contrast, this study's novel doping-free TiO_2 nanocomposite membranes achieved higher degradation efficiencies, reaching complete OFL removal in real wastewater and a maximum removal of 90% in synthetic wastewater for the initial 10 mg/L concentration of OFL in 240 minutes of UV exposure, using a much lower TiO_2 concentration of only 12.56 mg.

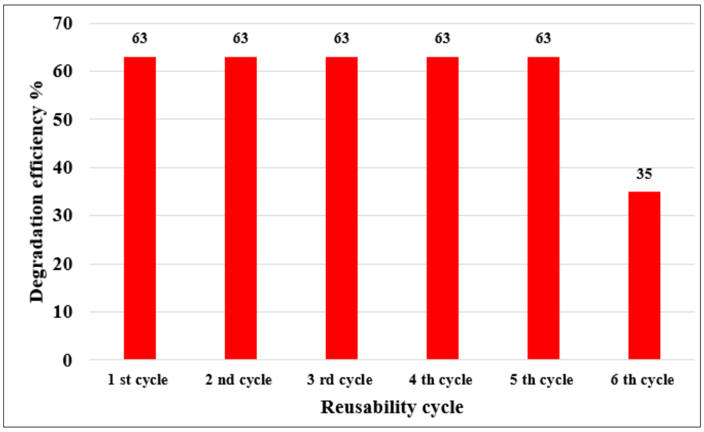

Figure 16: Reusability cycles of the nanocomposite membrane for the initial 3 mg/L concentration of OFL degradation.

4. Conclusion

This study proved that PSf/TiO_2 nanocomposite membrane manufactured via phase inversion method is a successful technique for the photocatalytic degradation of the commonly used antibiotic OFL from synthetic wastewater under UV-light. The photocatalytic degradation efficiency reached a complete drug removal in real wastewater and a maximum removal of 90% in synthetic wastewater for the initial 10 mg/L concentration of OFL. The photocatalytic performance was discovered to be affected by several operational parameters, such as temperature, catalyst concentration, irradiation time, initial pharmaceutical dosage, and pH of the solution. The optimum parameters for OFL removal were at pH of 6 for typical distilled water, a TiO_2 concentration of 12.56 mg, four PSf/TiO_2 (5 wt%) nanocomposite membranes with a total membrane surface area of 64 cm^2, a UV-light of 40 w, an ideal temperature (25 ± 2◦C), UV exposure time of 240 min, and 70 rpm.

The values of kinetic data were very well fitted by the PSO kinetic model for initial concentrations of OFL at 3, 5, 7, and 10 mg/L, while initial concentrations of 30, 50, and 70 mg/L were best fitted by the PFO kinetic model. The nanocomposite membranes' cross-sectional morphology demonstrated how well the TiO_2 NPs are embedded in the PSf polymer. The EDX spectra of all membrane samples revealed characteristic peaks for the PSf polymer, indicating the presence of sulfur, oxygen, and carbon as the dominant elements on their surfaces. Additionally, with PSf/TiO_2 (1,3, and 5 wt%) nanocomposite membrane, a peak of Ti was observed. According to the membrane stability and reusability investigation, the photocatalytic efficiencies of PSf/TiO_2 nanocomposite membrane remained steady and only declined during the 6th photocatalytic cycle. Accordingly, the proposed nanocomposite membrane proved to be a promising, efficient, and economic solution for degrading OFL pharmaceuticals with a lower catalyst loading and a shorter treatment time for OFL, compared to other membranes requiring the addition of dopants.

5. Conflicts of interest

"There are no conflicts to declare".

6. Formatting of funding sources

The authors declare that no funding was received for this work.

7. Acknowledgments

The authors of this research are thankful to Dr. Alaa Mohamed from the Section of Chemical Science and Engineering, Department of Chemistry and Bioscience, Aalborg University, Niels Bohrs Vej 8, Esbjerg 6700, Denmark, for his guidance and assistance in the fabrication and characterization of the nanocomposite membranes.

8. References

[1] Kumar S, Bhawna, Sharma R, Gupta A, Dubey KK, Khan AM, et al. TiO_2 based Photocatalysis membranes: An efficient strategy for pharmaceutical mineralization. Science of the Total Environment 2022;845. https://doi.org/10.1016/j.scitotenv.2022.157221.

[2] Ashraf M, Galal MM, Matta ME. Removal of danofloxacin and ofloxacin as different generations of fluoroquinolones from aqueous solutions through the adsorption process using granular activated carbon: A comparative study, mechanism elucidation, and applicability investigation. Alexandria Engineering Journal 2023;71:679–90. https://doi.org/10.1016/j.aej.2023.03.096.

[3] Peterson JW, Gu B, Seymour MD. Surface interactions and degradation of a fluoroquinolone antibiotic in the dark in aqueous TiO_2 suspensions. Science of the Total Environment 2015;532:398–403. https://doi.org/10.1016/j.scitotenv.2015.06.024.

[4] Ahmed R, gomaa alshimaa, elsisi amina, Elsayed A. apple peels as a natural adsorbent to remove antibiotics from wastewater. Egypt J Chem 2024;0:0–0. https://doi.org/10.21608/ejchem.2024.259896.9128.

[5] Hanif H, Waseem A, Kali S, Qureshi NA, Majid M, Iqbal M, et al. Environmental risk assessment of diclofenac residues in surface waters and wastewater: a hidden global threat to aquatic ecosystem. Environ Monit Assess 2020;192. https://doi.org/10.1007/s10661-020-8151-3.

[6] O'Flynn D, Lawler J, Yusuf A, Parle-Mcdermott A, Harold D, Mc Cloughlin T, et al. A review of pharmaceutical occurrence and pathways in the aquatic environment in the context of a changing climate and the COVID-19 pandemic. Analytical Methods 2021;13:575–94. https://doi.org/10.1039/d0ay02098b.

[7] Kaur A, Gupta G, Ibhadon AO, Salunke DB, Sinha ASK, Kansal SK. A Facile synthesis of silver modified ZnO nanoplates for efficient removal of ofloxacin drug in aqueous phase under solar irradiation. J Environ Chem Eng 2018;6:3621–30. https://doi.org/10.1016/j.jece.2017.05.032.

[8] Nassar HF, Shaban A, Zaher A, Abdelmonein T, Salama E, Gaber Y, et al. Iron-Trimesic Metal Organic Frameworks as Nano-Adsorbents for Tetracycline and Ceftriaxone Contaminated Wastewater Effluents. Egypt J Chem 2023;66:439–49. https://doi.org/10.21608/EJCHEM.2022.153568.6647.

[9] Frascaroli G, Reid D, Hunter C, Roberts J, Helwig K, Spencer J, et al. Pharmaceuticals in wastewater treatment plants: A systematic review on the substances of greatest concern responsible for the development of antimicrobial resistance. Applied Sciences (Switzerland) 2021;11. https://doi.org/10.3390/app11156670.

[10] Kaur M, Mehta SK, Kansal SK. Visible light driven photocatalytic degradation of ofloxacin and malachite green dye using cadmium sulphide nanoparticles. J Environ Chem Eng 2018;6:3631–9. https://doi.org/10.1016/j.jece.2017.04.006.

[11] Yang Q, Gao Y, Ke J, Show PL, Ge Y, Liu Y, et al. Antibiotics: An overview on the environmental occurrence, toxicity, degradation, and removal methods. Bioengineered 2021;12:7376–416. https://doi.org/10.1080/21655979.2021.1974657.

[12] Li L, He J, Gan Z, Yang P. Occurrence and fate of antibiotics and heavy metals in sewage treatment plants and risk assessment of reclaimed water in Chengdu, China. Chemosphere 2021;272. https://doi.org/10.1016/j.chemosphere.2021.129730.

[13] Peres MS, Maniero MG, Guimarães JR. Photocatalytic degradation of ofloxacin and evaluation of the residual antimicrobial activity. Photochemical and Photobiological Sciences 2015;14:556–62. https://doi.org/10.1039/c4pp00256c.

[14] Jia A, Wan Y, Xiao Y, Hu J. Occurrence and fate of quinolone and fluoroquinolone antibiotics in a municipal sewage treatment plant. Water Res 2012;46:387–94. https://doi.org/10.1016/j.watres.2011.10.055.

[15] Vasquez MI, Garcia-Käufer M, Hapeshi E, Menz J, Kostarelos K, Fatta-Kassinos D, et al. Chronic ecotoxic effects to Pseudomonas putida and Vibrio fischeri, and cytostatic and genotoxic effects to the hepatoma cell line (HepG2) of ofloxacin photo(cata)lytically treated solutions. Science of the Total Environment 2013;450–451:356–65. https://doi.org/10.1016/j.scitotenv.2012.05.096.

[16] Singh A, Ramachandran SK, Gumpu MB, Zsuzsanna L, Veréb G, Kertész S, et al. Titanium dioxide doped hydroxyapatite incorporated photocatalytic membranes for the degradation of chloramphenicol antibiotic in water. Journal of Chemical Technology and Biotechnology 2021;96:1057–66. https://doi.org/10.1002/jctb.6617.

[17] Khan AH, Khan NA, Ahmed S, Dhingra A, Singh CP, Khan SU, et al. Application of advanced oxidation processes followed by different treatment technologies for hospital wastewater treatment. J Clean Prod 2020;269. https://doi.org/10.1016/j.jclepro.2020.122411.

[18] Ouda M, Kadadou D, Swaidan B, Al-Othman A, Al-Asheh S, Banat F, et al. Emerging contaminants in the water bodies of the Middle East and North Africa (MENA): A critical review. Science of the Total Environment 2021;754. https://doi.org/10.1016/j.scitotenv.2020.142177.

[19] Badawy MI, Wahaab RA, El-Kalliny AS. Fenton-biological treatment processes for the removal of some pharmaceuticals from industrial wastewater. J Hazard Mater 2009;167:567–74. https://doi.org/10.1016/j.jhazmat.2009.01.023.

[20] Leyva-Díaz JC, Batlles-Delafuente A, Molina-Moreno V, Molina JS, Belmonte-Ureña LJ. Removal of pharmaceuticals from wastewater: Analysis of the past and present global research activities. Water (Switzerland) 2021;13. https://doi.org/10.3390/w13172353.

[21] Wang X, Zhao Y, Sun Y, Liu D. Highly Effective Removal of Ofloxacin from Water with Copper-Doped ZIF-8. Molecules 2022;27. https://doi.org/10.3390/molecules27134312.

[22] Qureshi T, Memon N, Memon SQ, Ashraf MA. Decontamination of ofloxacin: optimization of removal process onto sawdust using response surface methodology. Desalination Water Treat 2016;57:221–9. https://doi.org/10.1080/19443994.2015.1006825.

[23] Asadzadeh Patehkhor H, Fattahi M, Khosravi-Nikou M. Synthesis and characterization of ternary chitosan–TiO_2–ZnO over graphene for photocatalytic degradation of tetracycline from pharmaceutical wastewater. Sci Rep 2021;11. https://doi.org/10.1038/s41598-021-03492-5.

[24] Wang J, Wang S. Removal of pharmaceuticals and personal care products (PPCPs) from wastewater: A review. J Environ Manage 2016;182:620–40. https://doi.org/10.1016/j.jenvman.2016.07.049.

[25] Oturan MA, Aaron JJ. Advanced oxidation processes in water/wastewater treatment: Principles and applications. A review. Crit Rev Environ Sci Technol 2014;44:2577–641. https://doi.org/10.1080/10643389.2013.829765.

[26] Dekkouche S, Morales-Torres S, Ribeiro AR, Faria JL, Fontàs C, Kebiche-Senhadji O, et al. In situ growth and crystallization of TiO_2 on polymeric membranes for the photocatalytic degradation of diclofenac and 17α-ethinylestradiol. Chemical Engineering Journal 2022;427. https://doi.org/10.1016/j.cej.2021.131476.

[27] Eslami A, Amini MM, Yazdanbakhsh AR, Mohseni-Bandpei A, Safari AA, Asadi A. N,S co-doped TiO_2 nanoparticles and nanosheets in simulated solar light for photocatalytic degradation of non-steroidal anti-inflammatory drugs in water: a comparative study. Journal of Chemical Technology and Biotechnology 2016;91:2693–704. https://doi.org/10.1002/jctb.4877.

[28] Koe WS, Chong WC, Pang YL, Koo CH, Ebrahim M, Mohammad AW. Novel nitrogen and sulphur co-doped carbon quantum dots/titanium oxide photocatalytic membrane for in-situ degradation and removal of pharmaceutical compound. Journal of Water Process Engineering 2020;33. https://doi.org/10.1016/j.jwpe.2019.101068.

[29] Liu L, Chen Z, Zhang J, Shan D, Wu Y, Bai L, et al. Treatment of industrial dye wastewater and pharmaceutical residue wastewater by advanced oxidation processes and its combination with nanocatalysts: A review. Journal of Water Process Engineering 2021;42. https://doi.org/10.1016/j.jwpe.2021.102122.

[30] Scarpelli F, Mastropietro TF, Poerio T, Godbert N. Mesoporous TiO_2 Thin Films: State of the Art. Titanium Dioxide - Material for a Sustainable Environment, InTech; 2018. https://doi.org/10.5772/intechopen.74244.

[31] Dadvar E, Kalantary RR, Ahmad Panahi H, Peyravi M. Efficiency of Polymeric Membrane Graphene Oxide-TiO_2 for Removal of Azo Dye. J Chem 2017;2017. https://doi.org/10.1155/2017/6217987.

[32] Ahmadi M, Ramezani Motlagh H, Jaafarzadeh N, Mostoufi A, Saeedi R, Barzegar G, et al. Enhanced photocatalytic degradation of tetracycline and real pharmaceutical wastewater using MWCNT/TiO_2 nano-composite. J Environ Manage 2017;186:55–63. https://doi.org/10.1016/j.jenvman.2016.09.088.

[33] Devahasdin S, Fan C, Li K, Chen DH. TiO_2 photocatalytic oxidation of nitric oxide: Transient behavior and reaction kinetics. J Photochem Photobiol A Chem 2003;156:161–70. https://doi.org/10.1016/S1010-6030(03)00005-4.

[34] Hamrayev H, Korpayev S, Shameli K. Advances in Synthesis Techniques and Environmental Applications of TiO_2 Nanoparticles for Wastewater Treatment: A Review. Journal of Research in Nanoscience and Nanotechnology 2024;12:1–24. https://doi.org/10.37934/jrnn.12.1.124.

[35] Dong H, Zeng G, Tang L, Fan C, Zhang C, He X, et al. An overview on limitations of TiO_2-based particles for photocatalytic degradation of organic pollutants and the corresponding countermeasures. Water Res 2015;79:128–46. https://doi.org/10.1016/j.watres.2015.04.038.

[36] Chijioke-Okere MO, Adlan Mohd Hir Z, Ogukwe CE, Njoku PC, Abdullah AH, Oguzie EE. TiO_2/Polyethersulphone films for photocatalytic degradation of acetaminophen in aqueous solution. J Mol Liq 2021;338. https://doi.org/10.1016/j.molliq.2021.116692.

[37] Kaur R, Kaur A, Kaur R, Singh S, Bhatti MS, Umar A, et al. Cu-BTC metal organic framework (MOF) derived Cu-doped TiO_2 nanoparticles and their use as visible light active photocatalyst for the decomposition of ofloxacin (OFX) antibiotic and antibacterial activity. Advanced Powder Technology 2021;32:1350–61. https://doi.org/10.1016/j.apt.2021.02.037.

[38] Bouyarmane H, El Bekkali C, Labrag J, Es-saidi I, Bouhnik O, Abdelmoumen H, et al. Photocatalytic degradation of emerging antibiotic pollutants in waters by TiO_2/Hydroxyapatite nanocomposite materials. Surfaces and Interfaces 2021;24. https://doi.org/10.1016/j.surfin.2021.101155.

[39] Abid M, Makhoul E, Tanos F, Iatsunskyi I, Coy E, Lesage G, et al. N-Doped HNT/TiO_2 Nanocomposite by Electrospinning for Acetaminophen Degradation. Membranes (Basel) 2023;13. https://doi.org/10.3390/membranes13020204.

[40] Hoseini SN, Pirzaman AK, Aroon MA, Pirbazari AE. Photocatalytic degradation of 2,4-dichlorophenol by Co-doped TiO_2 (Co/TiO_2) nanoparticles and Co/TiO_2 containing mixed matrix membranes. Journal of Water Process Engineering 2017;17:124–34. https://doi.org/10.1016/j.jwpe.2017.02.015.

[41] Almutairi MM, Ebraheim EE, Mahmoud MS, Atrees MS, Ali MEM, Khawassek YM. Nanocomposite of TiO_2 @ Ni-or co-doped graphene oxide for efficient photocatalytic water splitting. Egypt J Chem 2019;62:1649–58. https://doi.org/10.21608/EJCHEM.2019.9722.1648.

[42] Bhatia V, Ray AK, Dhir A. Enhanced photocatalytic degradation of ofloxacin by co-doped titanium dioxide under solar irradiation. Sep Purif Technol 2016;161:1–7. https://doi.org/10.1016/j.seppur.2016.01.028.

[43] Barquín C, Vital-Grappin A, Kumakiri I, Diban N, Rivero MJ, Urtiaga A, et al. Performance of TiO_2-Based Tubular Membranes in the Photocatalytic Degradation of Organic Compounds. Membranes (Basel) 2023;13. https://doi.org/10.3390/membranes13040448.

[44] Kesting RE. PHASE INVERSION MEMBRANES. ACS Symposium Series, ACS; 1985, p. 131–64. https://doi.org/10.1021/bk-1985-0269.ch007.

[45] Zhang F, Zhang W, Yu Y, Deng B, Li J, Jin J. Sol-gel preparation of PAA-g-PVDF/TiO_2 nanocomposite hollow fiber membranes with extremely high water flux and improved antifouling property. J Memb Sci 2013;432:25–32. https://doi.org/10.1016/j.memsci.2012.12.041.

[46] Yang Y, Zhang H, Wang P, Zheng Q, Li J. The influence of nano-sized TiO_2 fillers on the morphologies and properties of PSF UF membrane. J Memb Sci 2007;288:231–8. https://doi.org/10.1016/j.memsci.2006.11.019.

[47] Kusworo TD, Susanto H, Aryanti N, Rokhati N, Widiasa IN, Al-Aziz H, et al. Preparation and characterization of photocatalytic PSf-TiO_2/GO nanohybrid membrane for the degradation of organic contaminants in natural rubber wastewater. J Environ Chem Eng 2021;9. https://doi.org/10.1016/j.jece.2021.105066.

[48] Li W, Liang R, Hu A, Huang Z, Zhou YN. Generation of oxygen vacancies in visible light activated one-dimensional iodine TiO_2 photocatalysts. RSC Adv 2014;4:36959–66. https://doi.org/10.1039/c4ra04768k.

[49] Jyothi MS, Nayak V, Padaki M, Balakrishna RG. Sunlight active PSf/TiO_2 hybrid membrane for elimination of chromium. J Photochem Photobiol A Chem 2017;339:89–94. https://doi.org/10.1016/j.jphotochem.2017.02.017.

[50] Moradihamedani P, Ibrahim NA, Yunus WMZW, Yusof NA. Study of morphology and gas separation properties of polysulfone/titanium dioxide mixed matrix membranes. Polym Eng Sci 2015;55:367–74. https://doi.org/10.1002/pen.23887.

[51] Ahmad J, Deshmukh K, Habib M, Hägg MB. Influence of TiO$_2$ Nanoparticles on the Morphological, Thermal and Solution Properties of PVA/TiO$_2$ Nanocomposite Membranes. Arab J Sci Eng 2014;39:6805–14. https://doi.org/10.1007/s13369-014-1287-0.

[52] Ali N, Said A, Ali F, Khan M, Sheikh ZA, Bilal M. Development and Characterization of Functionalized Titanium Dioxide-Reinforced Sulfonated Copolyimide (SPI/TiO$_2$) Nanocomposite Membranes with Improved Mechanical, Thermal, and Electrochemical Properties. J Inorg Organomet Polym Mater 2020;30:4585–96. https://doi.org/10.1007/s10904-020-01636-0.

[53] Simonin JP. On the comparison of pseudo-first order and pseudo-second order rate laws in the modeling of adsorption kinetics. Chemical Engineering Journal 2016;300:254–63. https://doi.org/10.1016/j.cej.2016.04.079.

[54] Jorfi S, Barzegar G, Ahmadi M, Darvishi Cheshmeh Soltani R, Alah Jafarzadeh Haghighifard N, Takdastan A, et al. Enhanced coagulation-photocatalytic treatment of Acid red 73 dye and real textile wastewater using UVA/synthesized MgO nanoparticles. J Environ Manage 2016;177:111–8. https://doi.org/10.1016/j.jenvman.2016.04.005.

[55] Mohamed A, Salama A, Nasser WS, Uheida A. Photodegradation of Ibuprofen, Cetirizine, and Naproxen by PAN-MWCNT/TiO$_2$–NH$_2$ nanofiber membrane under UV light irradiation. Environ Sci Eur 2018;30. https://doi.org/10.1186/s12302-018-0177-6.

[56] Parlayıcı Ş, Yar A, Avcı A, Pehlivan E. Removal of hexavalent chromium using polyacrylonitrile/titanium dioxide nanofiber membrane. Desalination Water Treat 2016;57:16177–83. https://doi.org/10.1080/19443994.2015.1077349.

[57] Hapeshi E, Achilleos A, Vasquez MI, Michael C, Xekoukoulotakis NP, Mantzavinos D, et al. Drugs degrading photocatalytically: Kinetics and mechanisms of ofloxacin and atenolol removal on titania suspensions. Water Res 2010;44:1737–46. https://doi.org/10.1016/j.watres.2009.11.044.

[58] Zeng M. Influence of TiO$_2$ surface properties on water pollution treatment and photocatalytic activity. Bull Korean Chem Soc 2013;34:953–6. https://doi.org/10.5012/bkcs.2013.34.3.953.

[59] Nguyen LT, Nguyen HT, Pham TD, Tran TD, Chu HT, Dang HT, et al. UV–Visible Light Driven Photocatalytic Degradation of Ciprofloxacin by N,S Co-doped TiO$_2$: The Effect of Operational Parameters. Top Catal 2020;63:985–95. https://doi.org/10.1007/s11244-020-01319-7.

[60] Kusworo T, Nugraheni RE, Aryanti N. The Effect of Membrane Modification Using TiO$_2$, ZnO, and GO Nanoparticles: Challenges and Future Direction in Wastewater Treatment. IOP Conf Ser Mater Sci Eng 2021;1053:012135. https://doi.org/10.1088/1757-899x/1053/1/012135.

[61] Bilal A, Yasin M, Akhtar FH, Gilani MA, Alhmohamadi H, Younas M, et al. Enhancing Water Purification by Integrating Titanium Dioxide Nanotubes into Polyethersulfone Membranes for Improved Hydrophilicity and Anti-Fouling Performance. Membranes (Basel) 2024;14. https://doi.org/10.3390/membranes14050116.

[62] Pedersen MLK, Jensen TR, Kucheryavskiy S V., Simonsen ME. Investigation of surface energy, wettability and zeta potential of titanium dioxide/graphene oxide membranes. J Photochem Photobiol A Chem 2018;366:162–70. https://doi.org/10.1016/j.jphotochem.2018.07.045.

[63] El Bekkali C, Bouyarmane H, Laasri S, Karbane M El, Saoiabi A, Laghzizil A. Sorption and photocatalytic degradation of ciprofloxacin and ofloxacin in aqueous suspensions of TiO$_2$ and ZnO catalysts. vol. 8. pp. 4902-4906 2017.